GAS-SURFACE IMPACT ON FLOWFIELD STRUCTURE OF LOW-DENSITY HYPERSONIC FLOW OVER FLAT-NOSE BODIES

Wilson F. N. Santos
National Institute for Space Research
Combustion and Propulsion Laboratory
12630-000 Cachoeira Paulista, SP, Brazil
wilson@lcp.inpe.br

Abstract. *This work describes a computational study on hypersonic flow past flat-nose leading edges at zero incidence. Effects of incomplete surface accommodation in rarefied flow on the flowfield structure have been investigated by employing the Direct Simulation Monte Carlo (DSMC) method in combination with the Cercignani-Lampis-Lord gas surface interaction model, which incorporates separate accommodation coefficients for the normal and tangential velocity components. The work is motivated by interest in assessing the overall performance of flat-nose leading edges in order to consider them as possible candidates for blunting geometries of hypersonic leading edges. The results presented highlight the sensitivity of the primary properties to changes on the gas-surface accommodation coefficients. It is found that the normal and tangential accommodation coefficients have different influence on velocity, density, pressure and temperature along the stagnation streamline ahead of the leading edges as well as on the profiles adjacent to the body surface.*

Keywords: *hypersonic flow, rarefied flow, DSMC, blunt leading edge, gas-surface interaction.*

1. Introduction

The problems related to the aerothermodynamics at high flight Mach numbers have recently received the attention of several investigations because of their importance in connection with hypersonic vehicles and re-entry problems. Hypersonic vehicles are generally characterized by slender bodies and sharp leading edges in order to achieve good aerodynamic properties like high lift and low drag. Nevertheless, at high Mach numbers, the vehicle leading edges should be sufficiently blunt in order to reduce the heat transfer rate to acceptable levels, and possibly to allow for internal heat conduction. The use of blunt-nose shapes tends to alleviate the aerodynamic heating problem since the heat flux for blunt bodies is far lower than that for sharply pointed bodies. Due mainly to manufacturing problems and the extremely high temperatures attained in hypersonic flight, hypersonic vehicles will have blunt nose, although probably slendering out at a short distance from the nose. In this connection, flat-nose leading edges (Santos, 2003) have been considered as especially promising bluntness for hypersonic configurations in order to provide the leading edge heating and manufacturing requirements. The flat-nose concept is based on the work of Reller (1957), who has pointed out that a method of designing low heat transfer bodies is devised on the premise that the rate of heat transfer to the nose will be low if the local velocity is low, while the rate of heat transfer to the afterbody will be low if the local density is low. A typical body resulting from this design method consists of a flat nose followed by a highly curved, but for the most part slightly inclined, afterbody surface.

The work of Santos (2003) on hypersonic flow past flat-nose leading edges has been concentrated primarily on the analysis of the flowfield structure by considering the diffuse reflection model as being the gas-surface interaction. The diffuse model assumes that the molecules are reflected equally in all directions, quite independently of their incident speed and direction. Nevertheless, as a space flight vehicle is exposed to a rarefied environment over a considerable time, a departure from the fully diffuse model is observed, resulting from the colliding molecules that clean the surface of the vehicle, which becomes gradually decontaminated. Molecules reflected from clean surfaces show lobular distribution in direction. The flux distribution of scattered molecules emitted from clean surfaces frequently has a lobular shape that is centered about an angle, which tends to approach the specular angle for very high energies and/or low angle of attack.

In an effort to obtain further insight into the nature of the flowfield structure of flat-nose leading edges under hypersonic transitional flow conditions, a parametric study is performed on these shapes with a great deal of emphasis placed on the gas-surface interaction effects. In this scenario, the primary goal of this paper is to assess the sensitivity of the flowfield structure to variations in the surface accommodation coefficients experienced by the leading edges by employing the Cercignani-Lampis-Lord (CLL) model (Lord, 1991). The CLL model, which incorporates independent accommodation coefficients for the normal and tangential velocity components, is implemented into the DSMC code, and simulations are performed by assuming two-dimensional rarefied hypersonic flow.

2. Body Shape Definition

The geometry of the leading edges considered in this work is the same as that presented in Santos (2003). The blunt shapes consist of a flat nose supplemented by an afterbody surface defined, in dimensionless form, by the following contour,

$$\bar{x} = \int_{\bar{y}=1}^{\bar{y}=\bar{y}_{max}} \sqrt{\bar{y}^k - 1} \, d\bar{y} \qquad \text{where } \bar{x} = x/y_{nose} \text{ and } \bar{y} = y/y_{nose} \qquad (1)$$

The flat-nose shapes are modeled by assuming a sharp leading edge of half angle θ with a circular cylinder of radius R inscribed tangent to the wedge. The flat-nose shapes, inscribed between the wedge and the cylinder, are also tangent to them at the same common point where they have the same slope angle. The circular cylinder diameter provides a reference for the amount of blunting desired on the leading edges. It was assumed a leading edge half angle of 10 deg, a circular cylinder diameter of 10^{-2}m and flat-nose thickness t/λ_∞ of 0.01, 0.1 and 1, where $t = 2y_{nose}$ and λ_∞ is the freestream mean free path. Figure 1(a) illustrates this construction for the set of shapes investigated. From geometric considerations, the exponent k in Eq. (1) is obtained by matching slope on the wedge, circular cylinder and on the body shapes at the tangency point. For dimensionless thickness t/λ_∞ of 0.01, 0.1 and 1, k corresponds to 0.501, 0.746 and 1.465, respectively. The common body height H and the body length L are obtained in a straightforward manner.
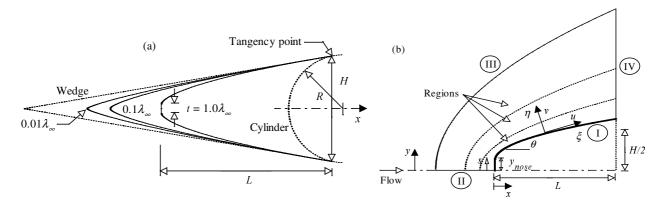

Figure 1: Drawing illustrating (a) the leading edge shapes and (b) the computational domain.

3. Computational Method and Procedure

In order to study rarefied flow with a significant degree of non-equilibrium, the Direct Simulation Monte Carlo (DSMC) method (Bird, 1994) is usually employed. The DSMC method has become the most common computational technique for modeling complex transitional flows of engineering interest. The DSMC method model a gas flow by using a computer to track the trajectory of simulated particles, where each simulated particle represents a fixed number of real gas particles. The simulated particles are allowed to move and collide, while the computer stores their position coordinates, velocities and other physical properties such as internal energy.

The molecular collisions are modeled by using the variable hard sphere (VHS) molecular model (Bird, 1981) and the no time counter (NTC) collision sampling technique (Bird, 1989). The energy exchange between kinetic and internal modes is controlled by the Borgnakke-Larsen statistical model (Borgnakke and Larsen, 1975). Simulations are performed using a non-reacting gas model consisting of two chemical species, N_2 and O_2. Energy exchanges between the translational and internal modes, rotational and vibrational, are considered. Relaxation collision numbers of 5 and 50 were used for the calculations of rotation and vibration, respectively.

In order to easily account for particle-particle collisions, the flowfield is divided into an arbitrary number of regions, which are subdivided into computational cells. The cells are further subdivided into subcells. In this fashion, the cell provides a convenient reference sampling of the macroscopic gas properties, while the collision partners are selected from the same subcell for the establishment of the collision rate. The computational domain used for the calculation is made large enough so that body disturbances do not reach the upstream and side boundaries, where freestream conditions are specified. A schematic view of the computational domain is depicted in Fig. 1(b). Side I is defined by the body surface. Reflection with incomplete surface accommodation is the condition applied to this side. Advantage of the flow symmetry is taken into account, and molecular simulation is applied to one-half of a full configuration. Thus, side II is a plane of symmetry. In such a boundary, all flow gradients normal to the plane are zero. At the molecular level, this plane is equivalent to a specular reflecting boundary. Side III is the freestream side through which simulated molecules enter and exit. Finally, the flow at the downstream outflow boundary, side IV, is predominantly supersonic and vacuum condition is specified (Bird, 1994). At this boundary, simulated molecules can only exit.

The numerical accuracy in DSMC method depends on the cell size chosen, on the time step as well as on the number of particles per computational cell. These effects were investigated in order to determine the number of cells and the number of particles required to achieve grid independence solutions. Grid independence was tested by running the calculations with half and double the number of cells in ξ and η directions (see Fig. 1(b)) compared to a standard grid.

Solutions (not shown) were near identical for all grids used and were considered fully grid independent.

In order to simulate the partial surface accommodation, the CLL model (Lord, 1991) was implemented into this DSMC calculation. The CLL model is derived assuming that there is no coupling between the normal and tangential momentum components. The two adjustable parameters appearing in the CLL model are the normal component of translational energy α_n and the tangential component of momentum σ_t expressed as being,

$$\alpha = \frac{e_i - e_r}{e_i - e_w} \qquad \sigma_t = \frac{\tau_i - \tau_r}{\tau_i} \qquad\qquad (2a, 2b)$$

where terms e and τ refer to the energy flux to the surface and the momentum flux acting tangential to the surface per unit area per unit time, respectively; subscripts i and r stand for the incident and reflected components, and w refers to the component that would be produced by a diffuse reflection at the temperature of the surface.

Nevertheless, in the implementation of the CLL model into the DSMC method, Bird (1994) has shown that it is equivalent to specify the normal α_n and tangential α_t components of translational energy, since $\alpha_t = \sigma_t (2-\sigma_t)$, and thus that $\sigma_t < \alpha_t$, assuming that σ_t lies between 0 and 1. In this work, the DSMC calculations were performed independently for three distinct numerical values for α_n and σ_t: 0.5, 0.75 and 1. It is important to mention that α_n and σ_t equal to 1 represent the diffusion reflection.

The freestream and flow conditions used in the present calculations are those given by Santos (2003) and summarized in Tab. 1. The freestream velocity V_∞, assumed to be constant at 3.56 km/s, corresponds to freestream Mach number M_∞ of 12. The translational and vibrational temperatures in the freestream are in equilibrium at 220 K, and the leading edge surface has a constant temperature T_w of 880 K for all cases considered.

Table 1: Freestream Conditions

Temperature T_∞ (K)	Pressure p_∞ (N/m^2)	Density ρ_∞ (kg/m^3)	Number density n_∞ (m^{-3})	Viscosity μ_∞ (Ns/m^2)	Mean free path λ_∞ (m)	Velocity V_∞ (m/s)
220.0	5.582	8.753 x 10^{-5}	1.8209 x 10^{21}	1.455 x 10^{-5}	9.03 x 10^{-4}	3560

The overall Knudsen number Kn_t, defined as the ratio of the freestream mean free path λ_∞ to the leading edge thickness t, corresponds to 1, 10 and 100 for leading edge thickness t/λ_∞ of 1, 0.1 and 0.01, respectively. The Reynolds number Re_t covers the range from 0.193 to 19.3, based on conditions in the undisturbed stream with leading edge thickness t as the characteristic length.

4. Computational Results and Discussion

The purpose of this section is to discuss and to compare differences in the flowfield properties due to variations on the surface accommodation coefficients and on the leading edge thickness. The flowfield properties of particular interest are velocity, density, pressure and temperature.

4.1. Velocity Profile

Normal velocity profiles along the stagnation streamline and their dependence on the normal and tangential accommodation coefficients are illustrated in Figs. 2(a-c) for leading edge thickness t/λ_∞ of 0.01, 0.1 and 1, which correspond to Kn_t of 100, 10 and 1, respectively. In this set of figures, the velocity ratio stands for the normal velocity v normalized by the freestream velocity V_∞, and the dimensionless height is the distance upstream the leading edges along the body normal (η) direction (see Fig. (1b)) normalized by the freestream mean free path λ_∞.

According to Figs. 2(a-c), it is seen that not only the leading edge thickness but also the partial surface accommodation influence the flowfield at the vicinity of the nose body. This domain of influence depends on both the leading edge thickness and the gas-surface interaction. The leading edge thickness effect results from the upstream diffusion of particles that are reflected from the nose of the leading edge. As a result, blunting the nose of the body (increasing t) leads to significantly larger disturbance upstream of the body. On the other hand, by altering the normal or tangential accommodation coefficient produces a substantial change in both incident and reflected molecular fluxes as the nose of the leading edge changes from sharp ($t/\lambda_\infty = 0.01$) to blunt ($t/\lambda_\infty = 1$) shape. It is also observed that the presence of the leading edge is propagated further upstream along the stagnation streamline by a reduction in the normal accommodation coefficient α_n. In contrast, molecules penetrate less upstream by a reduction in the tangential accommodation coefficient σ_t. For instance, the upstream disturbance for a velocity reduction of 1% ($v/V_\infty = 0.99$) is around $2.7\lambda_\infty$, $3.2\lambda_\infty$ and $5.1\lambda_\infty$ for cases $t/\lambda_\infty = 0.01$, 0.1 and 1, respectively, with diffuse reflection. However, it increases to around $3.4\lambda_\infty$, $4.8\lambda_\infty$ and $6.4\lambda_\infty$ for cases $t/\lambda_\infty = 0.01$, 0.1 and 1, respectively, and normal accommodation

coefficient α_n of 0.5. On the contrary, the upstream disturbance decreases to around $1.1\lambda_\infty$, $2.3\lambda_\infty$ and $4.7\lambda_\infty$ for cases $t/\lambda_\infty = 0.01$, 0.1 and 1, respectively, and tangential accommodation coefficient σ_t of 0.5.
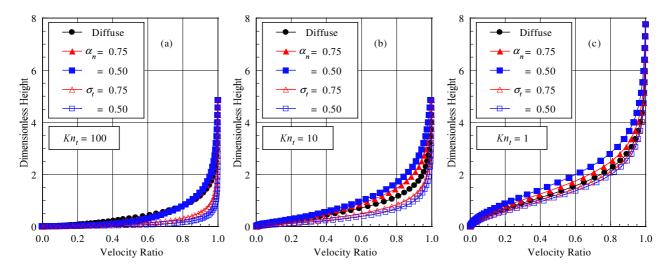

Figure 2: Normal velocity (v/V_∞) profiles along the stagnation streamline as a function of the accommodation coefficient for leading edges that correspond to thickness Knudsen number Kn_t of (a) 100, (b) 10 and (c) 1.

4.2. Density Profile

Density profiles along the stagnation streamline are plotted as a function of the normal and tangential accommodation coefficients in Figs. 3(a-c), for Kn_t of 100, 10 and 1, respectively. In this set of figures, dimensionless height is the distance in the normal body direction η normalized by λ_∞, and density ratio is the density ρ normalized by the freestream density ρ_∞.

The predictions of density for all cases investigated show no sign of a discrete shock wave. Instead, there is a continuous rise in density from the freestream to the nose of the leading edges, rising to well above the continuum inviscid limit for the majority of the cases. As a point of reference, the Rankine-Hugoniot relations give a postshock density that corresponds to the ratio $\rho/\rho_\infty = 5.8$ for freestream Mach number of 12. It can be also recognized that density rises gradually as the flow approaches the nose of the leading edge, indicating the diffuse nature of the shock wave, a characteristic of highly rarefied flows. Near the stagnation point ($\eta/\lambda_\infty \approx 0$), a substantial density increase occurs for full surface accommodation coefficient, i.e., for the diffuse reflection case that corresponds to α_n and σ_t equal to 1. This density increase is a characteristic of a cold-wall entry flow. In typical entry flow, the body surface temperature is low compared to the stagnation temperature. This leads to a steep density gradient near the body surface. For the present simulation, the ratio of wall temperature to stagnation temperature is 0.13, which corresponds to a cold-wall flow.
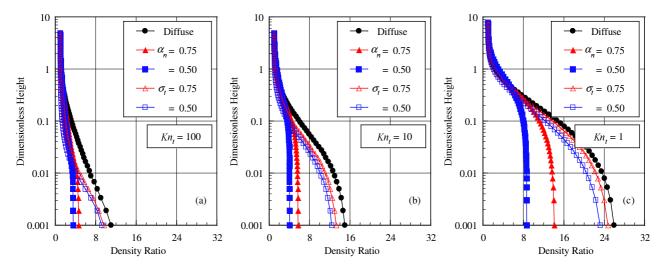

Figure 3: Density (ρ/ρ_∞) profiles along the stagnation streamline as a function of the surface accommodation coefficient for leading edges that correspond to thickness Knudsen number Kn_t of (a) 100, (b) 10 and (c) 1.

By examining the density profiles depicted in Figs. 3(a-c), it is observed that the normal and tangential accommodation coefficients produce different behaviors. These differing behaviors are caused basically by differences in the velocity distributions of the scattered molecules. When α_n and σ_t are equal to 1, the molecules reflect diffusely, which have a Maxwellian velocity distribution characteristic of the surface temperature. For a cold wall, the diffusely reflected molecules remain in the vicinity of the leading edge longer and result in a density buildup near the nose of the leading edge. However, when α_n and σ_t are different from 1, the CLL model provides a much complex description of the velocity distribution of scattered molecules in which the overall mean velocity and mean scattered angle are complex functions of the incoming velocity, surface temperature and the normal and tangential accommodation coefficients. For the surface accommodation coefficients less than one investigated, the CLL model gives a somewhat different mean velocity of scattered molecules and a distribution of scattered molecules tending to the specular angle. Consequently, molecules do not remain near the nose of the leading edge as long as with the diffuse reflection model, and lower density occurs near the nose of the leading edges.

Referring to Figs. 3(a-c), it may be recognized that, unlike normal velocity, density has little effect on the extent of the domain of influence upstream of the body for the leading edges investigated. Nevertheless, the extent of the flowfield disturbances becomes much larger as the leading edge becomes flatter. In addition, much of the density increase in the shock layer occurs after the temperature has reached its postshock value, as will be seen subsequently.

Figures 4(a-c) display selected profiles of the local density, expressed as a ratio to the freestream value ρ_∞, for three stations located on the afterbody surface for the $Kn_t = 10$ case ($t/\lambda_\infty = 0.1$ case). It is noted that density is affected by the surface accommodation coefficient, as would be expected. For the station corresponding to 80 deg, Fig. 4(a), the density variation is in excess of one order of magnitude for the tangential accommodation coefficient cases as well as for the diffuse case investigated. In this region, close to the stagnation region, the compression combined with a relatively cool wall produces a maximum density that is around 11 and 13.4 times the freestream value for σ_t of 0.75 and diffuse case, respectively. Because of the expansion along the body surface, the density adjacent to the surface decreases to around 7 and 6.6 times the freestream value for the same two cases, respectively, at the station corresponding to 20 deg, Fig. 4(c), a reduction around of 40%.
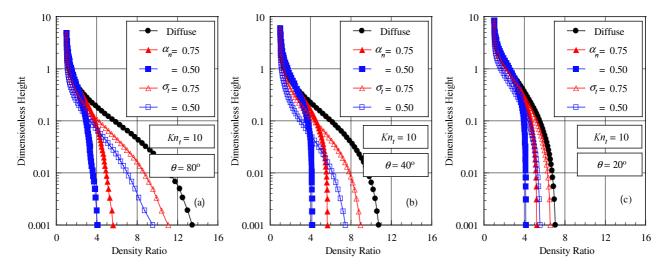

Figure 4: Density (ρ/ρ_∞) profiles along the body normal direction as a function of the surface accommodation coefficient for Knudsen number Kn_t of 10 at afterbody stations that correspond to (a) 80, (b) 40 and (c) 20 degrees.

4.3. Temperature Profile

The strong shock wave that forms ahead of a blunt leading edge at hypersonic flow converts part of the kinetic energy of the freestream air molecules into thermal energy. This thermal energy downstream of the shock wave is partitioned into increasing the translational kinetic energy of the air molecules, and into exciting of other molecular energy states such as rotation and vibration.

The effect of full and partial surface accommodation coefficients on the kinetic temperature profiles along the stagnation streamline is demonstrated in Figs. 5 and 6 for flat-nose leading edges corresponding to Kn_t of 100 and 1, respectively. In this set of figures, temperature ratio accounts for the kinetic temperatures normalized by the freestream temperature T_∞. It is apparent from these figures that thermodynamic non-equilibrium occurs throughout the shock layer, as shown by the lack of equilibrium of the translational and internal kinetic temperatures. Thermal non-equilibrium occurs when the temperatures associated with the translational, rotational, and vibrational modes of a polyatomic gas are different. The overall kinetic temperature shown is defined for a non-equilibrium gas as the weighted mean of the translational and internal temperature (Bird, 1994). The overall kinetic temperature is equivalent

to the thermodynamic temperature only under thermal equilibrium conditions. As a matter of fact, it should be noticed that the ideal gas equation of state does not apply to this temperature in a non-equilibrium situation.

Referring to Figs. 5 and 6, in the undisturbed freestream far from the body, the translational and internal temperatures have the same value and are equal to the thermodynamic temperature. Approaching the nose of the leading edge, the translational temperature rises to well above the rotational and vibrational temperatures and reaches a maximum value that is a function of the leading edge thickness as well as of the surface accommodation coefficient. Since a large number of collisions is needed to excite molecules vibrationally from the ground state to the upper state, the vibrational temperature increases much more slowly than rotational temperature, as observed in Fig. 6 for the bluntest ($Kn_t = 1$) case investigated. Still further downstream toward the nose of the leading edge, the translational temperature decreases and reaches a value on the wall that is above the wall temperature, resulting in a temperature jump as defined in continuum formulation. It is apparent from Figs. 5 and 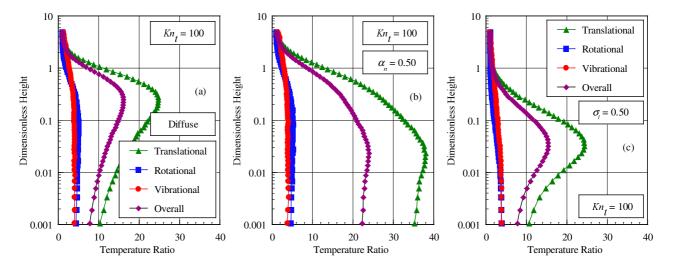6 that a reduction on the normal accommodation coefficient α_n causes a much more rise on the temperature jump than that on the tangential accommodation coefficient σ_t.
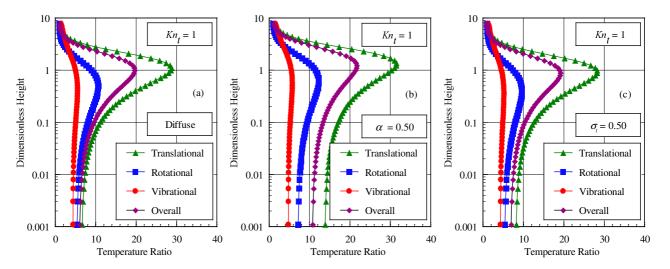

Figure 5: Kinetic temperature (T/T_∞) profiles along the stagnation streamline for leading edge that corresponds to thickness Knudsen number Kn_t of 100 for (a) diffuse case, (b) α_n of 0.5 and (c) σ_t of 0.5.

Figure 6: Kinetic temperature (T/T_∞) profiles along the stagnation streamline for leading edge that corresponds to thickness Knudsen number Kn_t of 1 for (a) diffuse case, (b) α_n of 0.5 and (c) σ_t of 0.5.

In what follows, it is instructive to note that the substantial rise in translational kinetic temperature for the leading edges occurred before the density rise (see Fig. 3). For instance, the kinetic translational temperature reaches the maximum value around a distance of one freestream mean free path from the nose of the leading edge for the $Kn_t = 1$ case, while the density ratio ρ/ρ_∞ is around 2.5 at the same station. The translational kinetic temperature rise for blunt leading edges results from the large velocity separation between the molecular sample consisting of mostly undisturbed freestream molecules with the molecules that have been affected by the shock and reflected from the body.

In order to bring out important features of the gas-surface interaction effects, particular attention is paid to the translational temperature in the shock layer. In this respect, the translational temperature variation is taken normal to the body surface at afterbody stations corresponding to 80, 40 and 20 degrees. Figures 7(a-c) depict profiles of translational temperatures at the considered positions normal to the body surface along the η-axis for the $Kn_t = 10$ case. According to this set of plots, it is clearly observed that the downstream evolution of the flow displays a smearing tendency of the shock wave due to the displacement of the maximum value for the translational temperature. Also, it may be recognized from the translational temperature distribution in Figs. 7(a-c) that significant changes in the translational temperature profiles occur within a thin layer adjacent to the body surface for the surface accommodation coefficient range investigated.
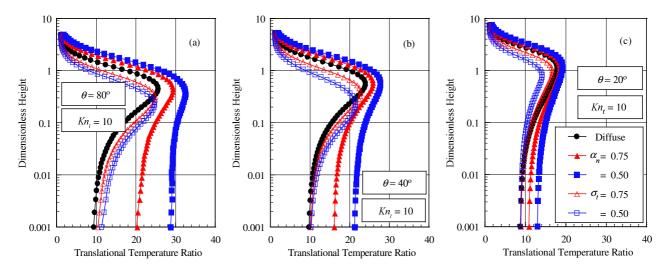

Figure 7: Translational temperature (T_T/T_∞) profiles along the body normal direction as a function of the surface accommodation coefficient for Kn_t of 10 at afterbody stations that correspond to (a) 80, (b) 40 and (c) 20 degrees.

4.4. Pressure Profile

The large amount of kinetic energy present in a hypersonic freestream is converted by molecular collisions into high thermal energy surrounding the body and by flow work into increased pressure. In this respect, the stagnation line is a zone of strong compression, where pressure increases from the freestream to the stagnation point due to the shock wave that forms ahead of the leading edges.

Representative pressure profiles along the stagnation streamline are shown as a function of the surface accommodation coefficients in Figs. 8(a-c) for Kn_t of 100, 10 and 1, respectively. In this set of diagrams, pressure ratio is the pressure p normalized by the freestream pressure p_∞. As can be seen, there is a continuous rise in pressure from the freestream up to the nose of the leading edge for the majority of the cases investigated. Near the stagnation point, a substantial pressure increase occurs with increasing the leading edge thickness t. It is apparent from these figures that the general shape of the pressure distribution profiles is not preserved when the surface accommodation coefficients change from 1 to 0.5. Pressure is given by the product of the density and the mean value of the square molecular velocity. As shown earlier, due to the normal or tangential accommodation coefficient reduction, density decreases and the translational kinetic temperature, which is associated to the motion of the molecules, increases in different ways. As pressure depends on these opposite behaviors, appreciable changes are observed in the pressure distribution along the stagnation streamline for the surface accommodation coefficient range investigated.

The extent of the upstream flowfield disturbance for pressure is significantly different from that for density. The domain of influence for pressure is higher than that for density and lower than that for temperature. Similar to the density, much of the pressure increase in the shock layer occurs after the translational kinetic temperature has reached its postshock value.

Local pressure, expressed as a ratio to the freestream value, for three stations located on the afterbody surface related to the $Kn_t = 10$ case ($t/\lambda_\infty = 0.1$ case) is illustrated in Figs. 9(a-c). It is apparent from these profiles that pressure is affected by diminishing the normal and tangential accommodation coefficients, as was mentioned earlier. For the station corresponding to 80 deg, Fig. 9(a), the pressure variation is in excess of two orders of magnitude for the accommodation coefficient range investigated. In this region, close to the stagnation region, the compression produces a maximum pressure that is around 125 times the freestream value for the cases investigated. Due to the expansion along the body surface, the pressure adjacent to the surface decreases to around 60 times the freestream value for the cases at the station corresponding to 20 deg, as shown Fig. 9(c). This corresponds a reduction around of 50% in pressure from station 80 to 20 degrees.
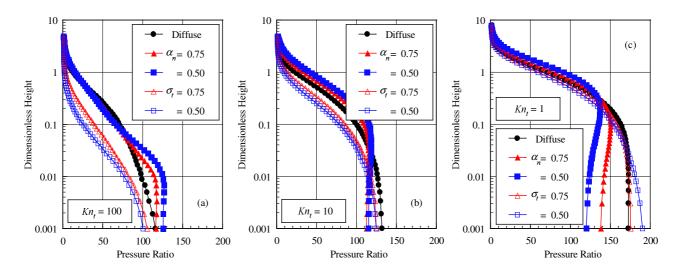
Figure 8: Pressure (p/p_∞) profiles along the stagnation streamline as a function of the surface accommodation coefficient for leading edges that correspond to thickness Knudsen number Kn_t of (a) 100, (b) 10 and (c) 1.
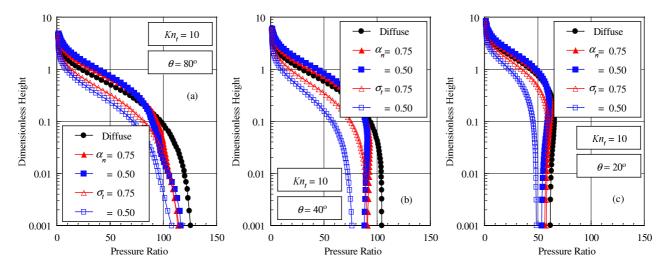

Figure 9: Pressure (p/p_∞) profiles along the body normal direction as a function of the surface accommodation coefficients for Knudsen number Kn_t of 10 at afterbody stations that correspond to (a) 80, (b) 40 and (c) 20 degrees.

5. Concluding Remarks

Computations of a rarefied hypersonic flow on blunt leading edges have been performed by using the Direct Simulation Monte Carlo method. The calculations provided information concerning the nature of the flowfield structure about the primary properties at the vicinity of the nose and immediately adjacent to the body surface for a family of contours composed by a flat nose followed by a highly curved afterbody surface.

Effects of gas-surface interaction on the velocity, density, pressure, and temperature for a representative range of parameters were investigated. Normal and tangential accommodation coefficients varied independently from 1 to 0.5. In addition to that, the leading edge nose thickness ranged from 0.01 to 1 of the freestream mean free path, corresponding thickness Knudsen numbers from 100 to 1. Cases considered in this study covered the hypersonic flow from the transitional flow regime to the free molecular flow regime.

It was found that changes on the shape of the leading edge as well as on the surface accommodation coefficients disturbed the flowfield far upstream, as compared to the freestream mean free path, and the domain of influence decreased by reducing the nose thickness, as the leading edge became sharp. The analysis also showed that the domain of influence decreased by reducing the tangential accommodation coefficient and increased by a reduction in the normal accommodation coefficient. Moreover, the extent of the upstream flowfield disturbance is significantly different for each one of the flow properties. The domain of influence for temperature is larger than that observed for pressure and density. Since the extent of the flowfield disturbance is significantly different for each one of the leading edge shapes, this will have important implications in problems that take into account for the gas-phase chemistry and for the gas-surface catalytic activity.

The effects of either normal or tangential accommodation coefficient showed that in order to make accurate predictions of the flowfield structure on bodies in rarefied hypersonic flow it would be necessary to take surface accommodation into account. The calculations presented in this work have only covered a limited number of parametric variations. Further calculations with additional combinations of normal and tangential accommodation coefficients or where the internal energy accommodation is varied independently might provide more insight into the sensitivity of the primary properties to gas-surface interaction model.

7. References

Bird, G. A., 1981, "Monte Carlo Simulation in an Engineering Context", Progress in Astronautics and Aeronautics: Rarefied gas Dynamics, Ed. Sam S. Fisher, Vol. 74, part I, AIAA New York, pp. 239-255.

Bird, G. A., 1989, "Perception of Numerical Method in Rarefied Gasdynamics", Rarefied gas Dynamics: Theoretical and Computational Techniques, Eds. E. P. Muntz, and D. P. Weaver and D. H. Capbell, Vol. 118, Progress in Astronautics and Aeronautics, AIAA, New York, pp. 374-395.

Bird, G. A., 1994, "Molecular Gas Dynamics and the Direct Simulation of Gas Flows", Oxford University Press, Oxford, England, UK.

Borgnakke, C. and Larsen, P. S., 1975, "Statistical Collision Model for Monte Carlo Simulation of Polyatomic Gas Mixture", Journal of computational Physics, Vol. 18, No. 4, pp. 405-420.

Lord, R. G., 1991, "Application of the Cercignani-Lampis Scattering Kernel to Direct Simulation Monte Carlo Method", Proceedings of the 17th International Symposium on Rarefied Gas Dynamics, edited by A. E. Beylich, Aachen, Germany, pp. 1427-1433, July 8-14.

Reller Jr., J. O., 1957, "Heat Transfer to Blunt Nose Shapes with Laminar Boundary Layers at High Supersonic Speeds", NACA RM-A57FO3a.

Santos, W. F. N., 2003, "Aerodynamic Heating on Blunt Nose Shapes in Rarefied Hypersonic Flow", Proceedings of the 17th International Congress of Mechanical Engineering, COBEM 2003, 10-14 Nov, São Paulo, SP, Brazil.